Frequency-Dependent Microstate Characteristics for Mild Cognitive Impairment in Parkinson's Disease

Chen Liu, *Member, IEEE*, Zhiqi Jiang, Shang Liu, Chunguang Chu, Jiang Wang, *Member, IEEE*, Wei Liu, Yanan Sun, Mengmeng Dong, Qingqing Shi, Pengcheng Huang, and Xiaodong Zhu

***Abstract*— Cognitive impairment is typically reflected in the time and frequency variations of electroencephalography (EEG). Integrating time-domain and frequency-domain analysis methods is essential to better understand and assess cognitive ability. Timely identification of cognitive levels in early Parkinson's disease (ePD) patients can help mitigate the risk of future dementia. For the investigation of the brain activity and states related to cognitive levels, this study recruited forty ePD patients for EEG microstate analysis, including 13 with mild cognitive impairment (MCI) and 27 without MCI (control group). To determine the specific frequency band on which the microstate analysis relies, a deep learning framework was employed to discern the frequency dependence of the cognitive level in ePD patients. The input to the convolutional neural network consisted of the power spectral density of multi-channel multi-point EEG signals. The visualization technique of gradient-weighted class activation mapping was utilized to extract the optimal frequency band for identifying MCI samples. Within this frequency band, microstate analysis was conducted and correlated with the Montreal Cognitive Assessment (MoCA) Scale. The deep neural network revealed significant differences in the 1-11.5Hz spectrum of the ePD-MCI group compared to the control group. In this characteristic frequency band, ePD-MCI patients exhibited a pattern of global microstate disorder. The coverage rate and occurrence frequency of microstate A and D increased significantly and were both negatively correlated with the MoCA scale. Meanwhile, the coverage, frequency and duration of microstate C decreased significantly and were positively correlated with the MoCA scale. Our work unveils abnormal microstate characteristics in ePD-MCI based on time-frequency fusion, enhancing our understanding of cognitively related brain dynamics and providing electrophysiological markers for ePD-MCI recognition.**

***Index Terms*— Deep neural network, frequency bands optimization, microstate, mild cognitive impairment, Parkinson's disease.**

I. Introduction

PARKINSON'S disease (PD) is the second most prevalent neurodegenerative disorder among the elderly [1]. Its motor symptoms, such as bradykinesia, rigidity, and resting tremor, alongside nonmotor dysfunctions like cognitive decline, depression, and anxiety, profoundly affect patients' daily lives [1], [2]. Clinical findings reveal that nearly a quarter of early PD (ePD) patients experience mild cognitive impairment (MCI) [3] and ePD patients with MCI are at an increased risk of developing dementia [4], [5], [6]. Unfortunately, there are currently no effective treatments for dementia of PD patients and once dementia symptoms emerge, deep brain stimulation (DBS) surgery becomes infeasible for managing motor symptoms. Moreover, the impact of cognitive impairment on brain activity of PD patients, particularly those in early stages, remains poorly understood, posing considerable challenges in the clinical identification of MCI during the ePD phase. Hence, it is of utmost importance to investigate the neural mechanism underlying ePD-MCI and identify reliable biomarkers to assist clinicians in diagnosing or monitoring patients at risk of mis- or missed-prognosis of PD-MCI [7].

Electroencephalography (EEG) is a non-invasive and cost-effective technique for recording the brain's electrical activity [8]. Among traditional EEG analysis methods,

Manuscript received 7 April 2023; revised 1 August 2023 and 7 September 2023; accepted 28 September 2023. Date of publication 13 October 2023; date of current version 24 October 2023. This work was supported in part by the National Natural Science Foundation of China under Grant 62173241, in part by the STI2030-Major Projects under Grant 2022ZD0205300, in part by the Tianjin Health Commission under Grant TJWJ2022MS004 and Grant 2023001, and in part by the Tianjin Municipal Science and Technology Commission under Grant 22YDTPJC00350. *(Corresponding authors: Chunguang Chu; Jiang Wang; Xiaodong Zhu.)*

This work involved human subjects or animals in its research. Approval of all ethical and experimental procedures and protocols was granted by the Medical Ethics Committee of Tianjin Medical University General Hospital under Approval No. IRB2022-KY-300.

Chen Liu, Zhiqi Jiang, Shang Liu, and Jiang Wang are with the School of Electrical and Information Engineering, Tianjin University, Tianjin 300072, China (e-mail: liuchen715@tju.edu.cn; jzhiqi_3030@tju.edu.cn; 2410734480@qq.com; jiangwang@tju.edu.cn).

Chunguang Chu is with the School of Electrical and Information Engineering, Tianjin University, Tianjin 300072, China, and also with the Institute of Science and Technology for Brain-Inspired Intelligence, Fudan University, Shanghai 200433, China (e-mail: ccg_tina@tju.edu.cn).

Wei Liu, Yanan Sun, Mengmeng Dong, Qingqing Shi, Pengcheng Huang, and Xiaodong Zhu are with the Department of Neurology, Tianjin Neurological Institute, Tianjin Medical University General Hospital, Tianjin 300052, China (e-mail: liuwei-third@163.com; lemonmuqiu@163.com; dongmmeng@tmu.edu.cn; shiqingqing1026@163.com; 15122151514@163.com; zxd3516@tmu.edu.cn).

This article has supplementary downloadable material available at https://doi.org/10.1109/TNSRE.2023.3324343, provided by the authors.

Digital Object Identifier 10.1109/TNSRE.2023.3324343

microstate analysis offers high temporal resolution (i.e., sub-second level) to explore brain dynamics [9], [10]. EEG microstates are defined as global patterns of scalp potential topographies derived from multi-channel EEG dynamic sequences, organized in a specific manner [11], and are believed to play a fundamental role in brain signal processing. Their disruptions can significantly impact cognitive states, so researchers frequently employ microstate analysis to investigate the pathological neural mechanisms underlying cognitive impairment [12], [13], and connections between microstates and cognition/perception have been established [14], [15]. Specific microstates reflecting abnormalities in brain dynamics and inherent characteristics (e.g., frequency or duration) are considered quantifiable markers for various neuropsychiatric disorders [16]. For instance, Lian et al. found specialized single transitions in microstate syntax in MCI and Alzheimer's disease [17]. However, the spatiotemporal microstate characteristics of ePD-MCI remain unknown. Furthermore, the selection of EEG frequency band directly influences microstate analysis results [18], [19]. Javed et al. noted limitations in full-band microstate analysis for capturing multiplex information flow in the human brain and emphasized the sensitivity of microstate analysis to the frequency band, potentially leading to conflicting results [18]. Another study also indicated that alterations of microstate characteristics in Alzheimer's disease and MCI may occur in specific frequency bands [19]. Thus, before performing microstate analysis on ePD-MCI patients, this study first identified the specific frequency band related to MCI to ensure the accuracy and validity of the microstate analysis results. Javed et al. also noted a significant correlation between microstates and power spectra, confirming that spectral powers in composite signals influence the local peaks in global field potential (GFP) [18]. Knowledge about the characteristics of abnormal power spectra in MCI disorders is insufficient, although Klassen et al. demonstrated that EEG spectral parameters could complement neurophysiological tests for assessing cognitive decline in patients with neurodegenerative disorders [20]. Studies have indicated that alterations in signal power in the theta and lower alpha bands 4-8 Hz and 8-10 Hz, respectively) could indicate cognitive states [21], [22], and the increase of quantitative EEG spectral powers below 8 Hz and decrease above 8 Hz were related to an increased risk of cognitive impairment in PD [23], [24]. However, a gap persists in linking the frequency characteristics and time domain properties of EEG microstates, which is crucial for addressing the challenge posed by the uncertainty of frequencies in EEG microstate recognition.

In recent years, an increasing number of researches have sought to leverage neural networks to "read" EEG data, particularly to "read" its frequency information. Convolutional neural network (CNN), as a prominent deep learning model, excels in capturing implicit features through its efficient spatial information recognition, making it widely applicable in diverse domains [25], such as speech recognition and the identification of pathological EEG characteristics. Moreover, EEG, as a multi-channel brain signal detection method, offers high temporal resolution and spatial scalp potential field characteristics. Hence, utilizing CNN to construct an input space that incorporates spatio-frequency information becomes crucial in identifying the frequency characteristics of PD-MCI. Moreover, activation maps [26], saliency maps [27] and other interpretability techniques suggest the potential of deep learning in exploring unknown characteristic frequency bands. Schirrmeister et al. [28] investigated CNN architectures designed for EEG decoding and demonstrated superior decoding performance compared to the widely used filter bank common spatial patterns algorithm. Their research revealed that CNNs could efficiently leverage spectral power modulations within specific frequency bands, showcasing the potential of combining CNN with advanced EEG-based visualization technology.

Thus, we present a novel framework to investigate frequency-dependent microstate characteristics related to mild cognitive impairment in PD based on deep learning. Initially, we propose employing the multi-channel and multi-point EEG power spectrum as input for a CNN to perform the classification task. By automatically extracting hidden features from the input data, the CNN model can accurately recognize ePD-MCI samples. Subsequently, we utilize the gradient-weighted class activation mapping method to identify the characteristic frequency band associated with ePD-MCI. Then, we conduct a characteristic-frequency-band-driven microstate analysis to explore dynamic state changes and brain activity characteristics in ePD-MCI. The scheme of our work is illustrated in Fig. 1, and the structure of this paper is as follows: Section II introduces materials and methods, presenting the CNN model and the microstate analysis algorithm. In Section III, we report the frequency-dependent microstate characteristics related to ePD-MCI. Section IV offers a comprehensive discussion of the findings. Finally, Section V presents the conclusion drawn from our study.

II. Materials and Methods

A. Information About Participants

In this study, we recruited forty patients with primary PD who were treated in Tianjin Medical University General Hospital (28 females: age range of 50-74 years old, mean age of 64 years old; 12 males: age range of 45-74 years old, mean age of 61 years old). All subjects were in the early stage of PD with Hoehn and Yahr (H&Y) staging scales ranging from 1 to 2.5, and they abstained from medication for at least 12 hours before the EEG data collection to minimize the potential influence of drugs on the results. None of the patients exhibited head tremor symptoms during the EEG signal collection process. The cognitive level of each patient was assessed using the Montreal Cognitive Assessment Scale (MoCA), which measures overall cognitive performance on a scale from 0 to 30, with lower scores indicating a higher degree of cognitive impairment. The MoCA test was performed by the same neurologist immediately after EEG acquisition, following standardized criteria. Based on their MoCA scores, the forty ePD patients were divided into two groups: the mild cognitive impairment group (ePD-MCI) consisting of 13 subjects with MoCA scores between 19-25, and the normal cognitive group (ePD-nMCI) comprising 27 subjects with MoCA scores between 26-30. Basic information about

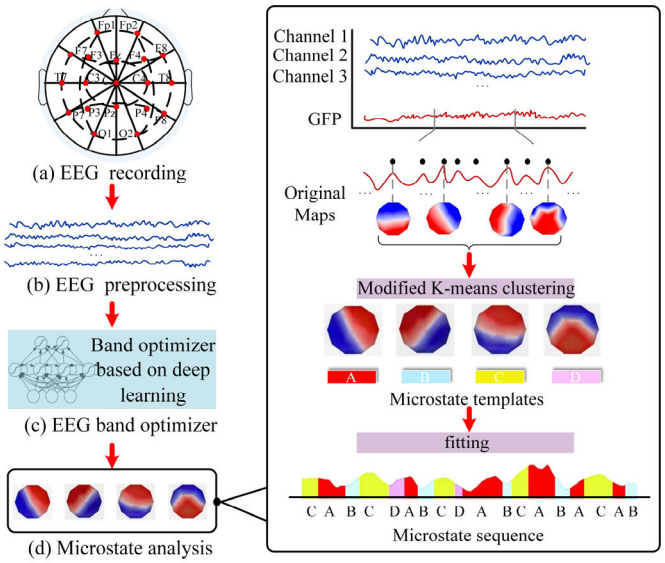

Fig. 1. The scheme of the study workflow. (a) EEG recording. (b) EEG preprocessing. (c) EEG band optimizer. (d) EEG microstate analysis. The lobal field power (GFP) of the EEG signal was calculated at each time point, and the corresponding electric potential distribution topography at the local peak point of GFP was obtained. The modified K-means clustering algorithm was employed to investigate EEG microstate classes on the group level. The four microstate templates were fit to original continuous EEG sequences on the individual level.

TABLE I
DESCRIPTION OF THE PATIENTS INCLUDED IN THE STUDY

Information	ePD-MCI (n=13, mean±S.D.)	ePD-nMCI (n=27, mean±S.D.)	Statistical test
Gender	6 males; 7 females	6 males; 21 females	$\chi 2 = 2.393$; $p = 0.122$
Age	62.000±8.347	63.778±5.727	$T = 0.790$; $p = 0.434$
H-Y stage	1.500±0.577	1.204±0.444	$T = -1.331$; $p = 0.191$
Course of the disease	3.385±2.725	4.130±3.994	$T = 0.606$; $p = 0.548$
MoCA scores	23.000±1.826	27.852±1.322	$T = 9.587$; $\mathbf{p < 0.001}$

Course of the disease referred to the time between subjects were diagnosed with PD and the EEG acquisition of this time, which was given in yearly units. χ^2 and t values were the statistical value obtained by chi-square test and two-sample t-test respectively. P values were the probability obtained by the corresponding statistical test method. Bold font represented significant differences.

the included patients is presented in Table I. In this table, $p < 0.05$ indicates statistically significant differences between groups. This research was conducted with the approval of the local ethics committee, and informed consent was obtained from all subjects in accordance with the Helsinki Declaration.

B. EEG Acquisition and Processing

All subjects remained seated calmly in a dimly lit room, closing their eyes while staying awake. Resting EEG signals were recorded using 19 Ag/AgCl scalp electrodes (SYMTOP, Beijing, China) placed according to the international 10-20 system of Electrode. Additional channels were set to record electrooculogram (EOG), electromyogram (EMG) from the skin between the thumb and index finger on the back of both hands, and electrocardiogram (ECG) signals. These additional channels were used to monitor eye movement, muscle activity, and heart activity, respectively, and to facilitate artifact removal. The sampling time of each subject was at least 15 minutes, with a sampling frequency of 500Hz. The impedances of all electrodes used for recording were maintained below 5kΩ.

To eliminate high-frequency interference and retain the relevant spectrum in the range of 1-45Hz, zero-phase shift filtering was employed. Subsequently, the continuous EEG signals from each channel were processed through the fast Independent Component Analysis (fastICA) algorithm [29], which decomposed the 19-channel EEG signals into statistically independent components (ICs). Pearson correlation was then calculated between the extracted ICs and the left and right EOG, EMG, and ECG signals. ICs with an absolute value of correlation coefficient greater than 0.5, indicating significant correlation with specific artifact signals, were zeroed out to remove artifacts. Afterward, experienced researchers carefully examined the noiseless EEG data to identify any other artifacts resulting from external factors, such as out-of-contact electrodes and body movements. Epochs with high amplitudes ($>80\mu$V) were tagged and rejected [30]. Preprocessing of the EEG data was performed using the EEGlab toolbox in MATLAB software (MathWorks Inc., Natick MA, United States). Finally, approximately 3 minutes continuous EEG recordings of each subject were retained for following analysis. This preprocessing protocol ensured the quality and reliability of the EEG data for subsequent investigations.

C. Microstate Analysis

The Cartool software was employed to conduct microstate analysis on clear EEG signals, each approximately 3 minutes in length for every patient, in four sequential steps, as illustrated in Fig. 1(d). In the first step, the global field power (GFP) of the EEG signal at each time point was calculated using formula (1) based on the EEG data of each subject. This provided an indicator reflecting the event-related global brain response and describing the corresponding rapid changes in brain activities.

$$GFP(t) = \sqrt{\frac{\sum_{i=1}^{n} [v_i(t) - \overline{v}(t)]^2}{n}} \quad (1)$$

where, n represented the number of electrodes, $v_i(t)$ represented the potential value of the ith electrode at time t, and $\overline{v}(t)$ represented the average potential value of all electrodes at time t. The second step involved obtaining the corresponding electric potential distribution topography at the local peak point of GFP. Given that the signal-to-noise ratio of EEG signals was highest at the local peak point of GFP, and the distribution of potential topographic map near it was stable [31], the topographic map at the GFP peak point was employed

to represent the surrounding brain activities. Both the first and second steps were performed on the individual level. In the third step, an improved K-means clustering algorithm was applied to the collection of topographic maps acquired from step two for all participants. This resulted in a set of EEG microstates applicable to all subjects. Previous studies using the K-means clustering algorithm suggested that the optimal number of clusters within subjects was four, which was further verified by the cross-validation (CV) criterion [32], [33]. To enhance the credibility of the chosen cluster number, we set the number of the clusters within a wide range, between two and six. Additionally, to address the uncertainty caused by the random selection of templates during the initialization process in k-means clustering, we conducted 100 random trail runs to minimize the run-to-run variance. Based on the maximum global explained variance (GEV), we determined an optimal set of four classes. We labeled the four microstate classes clustered from topographic maps of all patients as A, B, C, and D. The continuous EEG sequences of each subject were described by microstate series composed of these four microstate templates.

Finally, microstate time series were obtained for all 40 patients at the individual level. These microstate time series provided abundant parameters of potential neurophysiological relevance, and changes in these parameters can describe changes in brain state [34]. Three parameters were calculated from the microstate time series: (1) Mean Microstate Duration (MMD), representing the average length of time a given microstate remains stable; (2) Occurrence Per Second (OPS), indicating the average number of times per second that a specific microstate becomes dominant during the recording period; (3) Ratio of Time Coverage (RTC), characterizing the fraction of total recording time occupied by a given microstate.

D. Frequency Band Optimization Based on Deep Neural Network

The above microstate analysis relies on specific frequency bands. To determine the characteristic frequency bands for microstate analysis in ePD-MCI, we propose a frequency band optimization based on deep neural network, establishing a CNN model. The EEG data of each subject were divided into 130 data segments, each comprising a continuous 3-second sequence. Power spectral density (PSD) was calculated at 89 frequency points ranging from 1 to 45 Hz with a step size of 0.5 Hz for 19 EEG channels of all subjects using the P-welch function in MATLAB. These segments were defined as samples, resulting in a size of 89 × 19 for each sample, as depicted in Fig. 2(a). Thus, 130 samples from each subject were prepared for subsequent CNN model classification. We provided visualizations of these input data for CNN model in Figures S1 and S2 in Supplementary Material.

To avoid overfitting, we adopted a three-layer convolutional layer structure, commonly used in the literature, as shown in Fig. 2(b) [35]. The kernel size of the convolutional layer was set to 3 × 3. Batch normalization layers were included between convolutional layers to aid convergence and prevent overfitting. Additionally, the Rectified Linear Unit (ReLU) activation function was utilized. The model concluded with

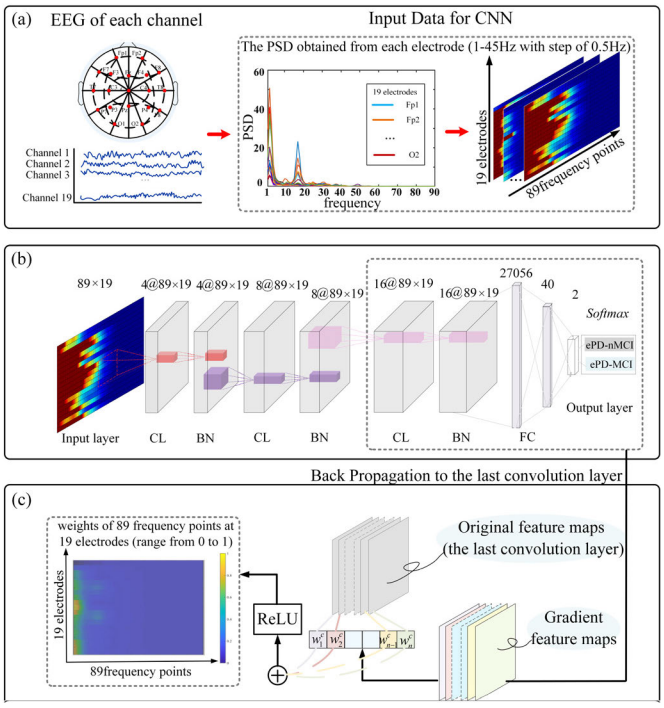

Fig. 2. Deep neural network. (a) Data preparation and representation. (b) CNN structure. The hidden layer of the CNN model in this work was designed with a three-layer convolution. CL: Convolution layer; BN: Batch normalization; FC: fully connected layer; 4@89 × 19: Four convolution kernels were used to extract characteristics from the input with dimensions 89 × 19. (c) Procedure of Gradient-weighted Class Activation Map (Grad-CAM).

two fully connected layers (the first layer with 27,056 neurons and the second layer with 40 neurons) to effectively capture nonlinear information. The softmax function mapped the values of neurons in the output layer to a range of 0 to 1, providing the probability of each output result.

The datasets for the two groups (ePD-MCI and ePD-nMCI) comprised a total of 5200 samples (40 subjects with 130 samples each). The dataset was randomly shuffled and divided into a training set and a testing set in a 4:1 ratio. To evaluate the model's performance, we conducted five-fold cross-validation by randomly dividing all samples into five equal sub-sample sets. During each training process, four sub-sample sets were used for training, and the remaining set was utilized for testing. The learning rate was set to 0.001. Accuracy (ACC) and the area under the curve (AUC) were calculated to assess the overall performance of the CNN model. ACC represents the percentage of correctly identified subjects, and AUC is the area under the receiver operating characteristic (ROC) curve, reflecting the probability that a positive sample (ePD-nMCI) is identified with a higher score than a negative sample (ePD-MCI) when randomly selected. Higher ACC and AUC values indicate better performance in ePD-MCI recognition. The formulas used for calculation are as follows:

$$ACC = \frac{TP + TN}{TP + TN + FP + FN} \times 100\% \tag{2}$$

$$AUC = \frac{\sum_{i \in positiveClass} rank_i - \frac{M(1+M)}{2}}{M \times N} \tag{3}$$

where TP represents a positive sample correctly identified as positive, TN represents a negative sample correctly identified as negative, FP represents a negative sample incorrectly identified as positive, and FN represents a positive sample incorrectly identified as negative. M and N represent the number of positive and negative samples, respectively, and $rank_i$ represents the serial number of the ith sample (sample probability scores are arranged from small to large).

The activation feature map of the last convolutional layer of the CNN model contained spatial information. The classification result for ePD-MCI and ePD-nMCI was determined by the weight of each feature layer in this layer. To visualize the model, we employed gradient-weighted class activation mapping (Grad-CAM) [36], as shown in Fig. 2(c). Specifically, we calculated the gradient feature maps and the weights of each feature in the last convolutional layer through backpropagation [37]. By taking a weighted sum, followed by a ReLU function, we obtained pixels positively affecting classification. This process resulted in activation feature maps comprising 89 frequency points, containing key features to accurately distinguish ePD-MCI and ePD-nMCI. The formulas used are shown below:

$$w_k^c = \frac{1}{Z}\sum_x\sum_y \frac{\partial Y^c}{\partial f_k(x,y)} \tag{4}$$

$$L^c_{Grad-CAM} = \mathrm{ReLU}\left(\sum_k w_k^c f_k(x,y)\right) \tag{5}$$

where $f_k(x, y)$ represents the feature graph obtained by the kth convolution kernel in the last convolution layer, with x and y indicating the coordinates of elements in the feature map. w_k^c denotes the "contribution" of the kth feature map to the classification of class C, Y_c represents the score of class C, and Z represents the size of the feature map. After obtaining the characteristic frequency band through the Grad-CAM algorithm, we re-filtered EEG signals to the optimal frequency band range for subsequent microstate analysis.

E. Statistical Analysis

The chi-square test was utilized to compare the gender distribution between the ePD-MCI and ePD-nMCI groups. Additionally, the two-sample t-test ($p < 0.05$) was conducted to assess the differences in microstate parameters, subject ages, H-Y stages, courses of the disease, and MoCA scores between the ePD-MCI and ePD-nMCI groups. Furthermore, Spearman correlation analysis was employed to evaluate the relationship between the obtained parameters and MoCA scores at a significant level of 0.05. To account for multiple comparisons, the False Discovery Rate correction (FDR) was applied. The statistical analyses were performed using the social science statistical software SPSS (25.0).

III. Results

A. Optimal Frequency Band Acquisition Based on Deep Neural Network

After employing the Grad-CAM algorithm to visualize the last convolutional layer of the CNN, we standardized the Grad-CAM results on a scale of 0 to 1 and represented them as brain topographic maps, as illustrated in Fig. 3. Among the 89 frequency points, 22 showed significant contributions in distinguishing between ePD-MCI and ePD-nMCI with standardized values greater than 0.2, while the remaining frequency points had minimal impact. Notably, these frequency points with the largest contribution were within the 1-11.5Hz range, indicating pronounced abnormal brain rhythm indicators in ePD-MCI compared to ePD-nMCI. The topographic maps of the 22 frequency bands highlighted specific brain regions associated with ePD-MCI, including the left temporal lobe, frontal lobe and occipital lobe, with particular emphasis on the left superior temporal gyrus and occipital lobe.

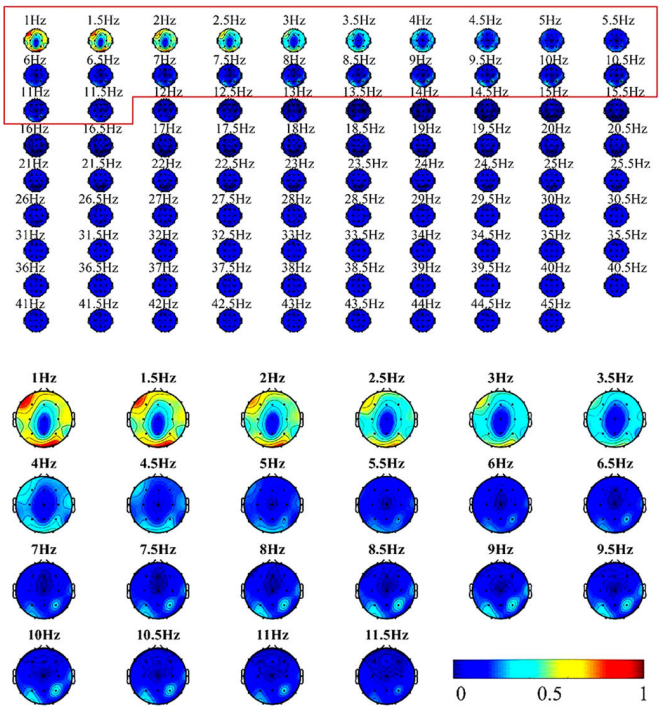

Fig. 3. Twenty-two frequency points with the largest contribution are in the range of 1 Hz to 11.5 Hz. The color in the brain topographic maps represents the weight of the identification region in the input space for identifying ePD-MCI.

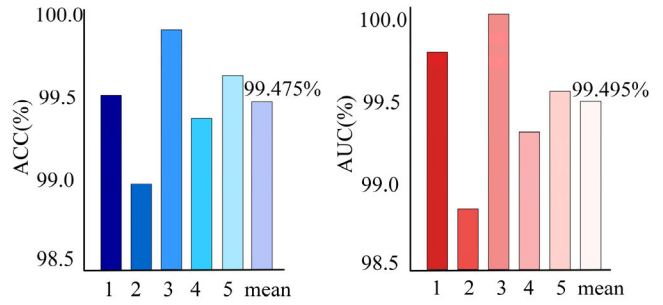

Fig. 4. Performance of CNN model. (a) The ACC of CNN models. (b) The AUC of CNN models. Each of the first five different color columns represents the result of a specific cross-validation fold of the model. The last color column represents the overall performance of the model, which is the average of the results from the five cross-validation folds.

The results of the five-fold cross-validation of the CNN model on the test sets are depicted in Fig. 4. The model demonstrated high accuracy in distinguishing between

TABLE II
MICROSTATE CHARACTERISTIC PARAMETERS AND DIFFERENCES BETWEEN GROUPS. (1 HZ - 11.5 HZ)

Parameter	Class	ePD-MCI (mean±S.D.)	ePD-nMCI (mean±S.D.)	Statistical test
MMD	A	55.20±1.43	52.30±5.51	T = -1.85; p = 0.10
	B	53.66±3.17	56.49±6.33	T = 1.51; p = 0.14
	C	45.41±2.01	51.52±5.07	**T = 4.16; p < 0.01**
	D	49.05±3.88	46.77±2.78	T = -2.14; p = 0.08
RTC	A	0.32±0.03	0.25±0.08	**T = -3.33; p < 0.01**
	B	0.30±0.04	0.32±0.07	T = 0.99; p = 0.33
	C	0.13±0.03	0.22±0.07	**T = 4.49; p < 0.01**
	D	0.18±0.05	0.14±0.04	**T = -3.24; p < 0.01**
OPS	A	2.48±0.15	1.98±0.45	**T = -3.77; p < 0.01**
	B	2.35±0.18	2.36±0.29	T = 0.08; p = 0.94
	C	1.27±0.28	1.86±0.39	**T = 4.86; p < 0.01**
	D	1.61±0.27	1.27±0.29	**T = -3.51; p < 0.01**

p values are corrected by FDR. Bold font represents significant differences.

ePD-MCI and ePD-nMCI, achieving an overall ACC of 99.475% ± 0.3236% (lowest ACC: 99.1514%; highest ACC: 99.7986%;) and AUC of 99.495% ± 0.4400% (lowest AUC: 99.055%; highest AUC: 99.935%;). These results indicate the excellent performance of the CNN model that we designed.

B. Characteristic Frequency Driven Microstate Analysis

After identifying the 1-11.5Hz EEG components as the characteristic frequency band with the largest differences between ePD-MCI and ePD-nMCI groups, we proceeded to re-filter the EEG signals of each subject, including only data within the characteristic frequency band, for the EEG microstate analysis. Within this characteristic frequency band, topographic maps of the two groups were clustered into four microstate classes (A, B, C, and D), as depicted on the left side of Fig. 5.

The microstate parameters and their statistics are presented in Fig. 5 and Table II. In the ePD-MCI group, the mean values of MMD, OPS and RTC for microstate classes A and D were higher compared to those in the ePD-nMCI group, while these parameters for microstate classes B and C were lower in the ePD-MCI group. A two-sample t-test was utilized to assess the differences between the two groups, revealing significant differences in all three microstate characteristic parameters.

The MMD of the four microstate classes ranged from 45.41ms to 56.49ms in both groups. The results of the two-sample t-test demonstrated that the MMD of microstate class C significantly decreased in the ePD-MCI group ($p < 0.001$). The RTC of the four microstate classes ranged from 13.00% to 32.00% in both groups. The two-sample t-test results indicated that compared to ePD-nMCI patients, ePD-MCI patients exhibited significantly increased time coverage in microstate B and D ($p = 0.0033$), while showing significantly decreased time coverage in microstate C ($p < 0.001$). The OPS of the four microstate classes ranged from 1.27 to 2.48 maps/s in both groups. Additionally, compared to ePD-nMCI patients, the frequency of microstate class C significantly decreased in ePD-MCI patients ($p < 0.001$), while microstate classes A and D were significantly increased ($p < 0.001$). These significant changes in microstate parameters reflect alterations in brain dynamics and hold the potential as promising biomarkers for ePD-MCI, aiding in auxiliary diagnosis. Furthermore, the results of microstate analysis based on the 1-45 Hz frequency band and within the 12-22.5 Hz frequency band can both be found in the Supplementary Material.

C. Correlation Between Microstate Temporal Parameters and Cognitive Level

The results of the Spearman correlation analysis between MoCA scores and all microstate characteristic parameters of microstate classes A to D in ePD patients are presented in Fig. 6. It is essential to note that lower MoCA scores indicate more severe cognitive impairment in ePD. Additionally, p-values were adjusted using FDR. The findings revealed significant negative correlations between the OPS and RTC of microstate class A with MoCA scores (OPS: $p = 0.0032$, $r = -0.4826$; RTC: $p = 0.0070$, $r = -0.4516$). Similarly, the OPS and RTC of microstate class D were significantly negatively correlated with MoCA scores (OPS: $p = 0.0053$, $r = -0.4449$; RTC: $p = 0.0127$, $r = -0.4052$). In contrast, a significant positive correlation was observed between the MMD, RTC and OPS of microstate class C with MoCA scores (MMD: $p = 0.0018$, $r = 0.4789$; RTC: $p = 0.0034$, $r = 0.5036$; OPS: $p = 0.0021$, $r = 0.5231$). No other significant correlations were observed between MoCA and other parameters. In essence, as the cognitive ability in ePD declined (as indicated by lower MoCA), the MMD and RTC of microstate classes A and D increased, while MMD, RTC and OPS of microstate class C decreased. These findings strongly suggest that changes in microstate characteristic parameters effectively reflect changes in the cognitive level of ePD patients.

IV. DISCUSSIONS

In this study, we designed a high spatio-frequency resolution CNN input and trained a CNN model to identify the characteristic frequency band associated with ePD-MCI. Through microstate analysis in specific frequency bands obtained by deep learning, we delved into the spatiotemporal characteristics of microstates, revealing abnormal brain temporal and spatial dynamics in ePD-MCI patients at a sub-second scale. Importantly, these findings establish a significant correlation between these microstate characteristics and cognitive function in ePD patients.

The visualization results from the CNN model highlighted that anomalies in ePD-MCI were predominantly distributed within the 1-11.5Hz frequency band, with delta and low alpha frequency bands showing higher weights than other bands. Concurrently, we found the left temporal lobe to be the most distinct characteristic region for ePD-MCI. Remarkably, our observations are consistent with those from Mostile's study, where quantitative EEG analysis demonstrated significant changes in delta PSD over the left temporal region and alpha PSD over the occipital regions in ePD-MCI compared to ePD-nMCI [38], providing additional support for our research. Abnormal slow rhythms within the delta frequency band,

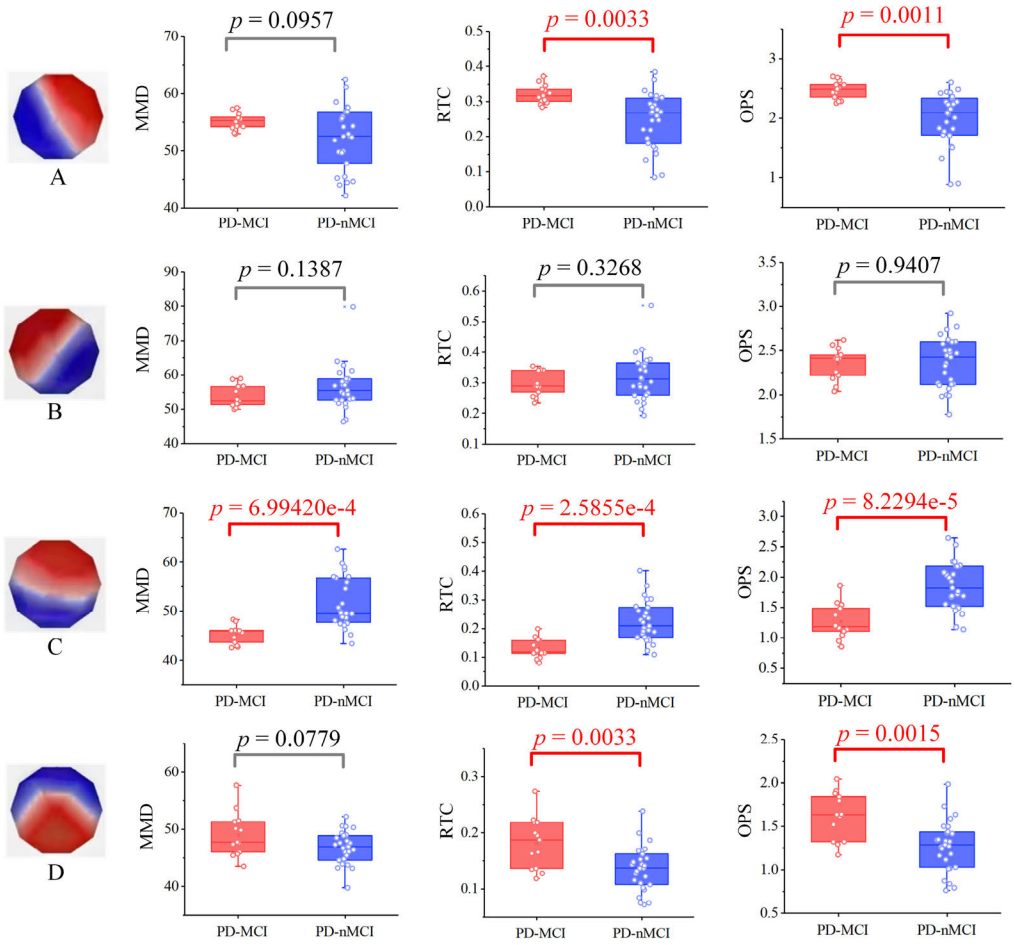

Fig. 5. Microstate characteristic statistics. Each column represents each microstate parameters (Column 1: MMD; Column 2: RTC; Column 3: OPS). Each line represents each microstate classes (Line 1: A Class; Line 2: B Class; Line 3: C Class; Line 4: D Class;). Significant differences between groups are indicated by red font. For multiple comparisons, FDR correction is performed for *p* values.

which intensify with declining cognitive ability, have been reported in several studies [39], [40]. Additionally, Jeong et al., found a decrease in alpha band PSD in the occipital region among subjects experiencing subjective cognitive decline [41]. Moreover, Mostile's study revealed significantly increased networks involving delta activity over the frontal lobe and decreased networks involving theta and delta activity over the parietal lobe in ePD-MCI patients compared to ePD-nMCI patients [38]. Similarly, Simon et al. reported higher power in delta frequency bands to be associated with greater cognitive impairment affecting memory, language, attention, and overall cognition function [42]. These consistent findings from previous studies further validate the presence of abnormalities in characteristic frequency bands in ePD-MCI patients.

While microstate analysis provides valueble insights into temporal dynamics, its relationship with frequency contents remains to be determined. Most previous studies using the microstate method to study MCI selected specific EEG frequency bands based on earlier references to microstate analysis [13], [17], [43]. However, this approach lacks a clear rationale for frequency band selection, and the amalgamation of EEG signals from different bands affects microstate temporal sequences and spatial configuration differently [18]. A study by Widmann et al. highlighted the limitations of wide bandwidth filtering, which may lead to inaccurate results in microstate analysis due to power accumulation from uninterested frequencies [44]. Other research by Musaeus et al. suggested that alterations in microstate patterns indicated disruptions in large-scale cortical networks in Alzheimer's Disease and MCI, which were associated with specific frequency bands [19]. Furthermore, the correlation between EEG power spectrum and microstate characteristics has been explored in studies by *Zulliger* et al. and *Liang* et al., emphasizing the potential of frequency-dependent EEG microstate analysis in understanding local patterns of brain activation and cognitive abilities [45], [46]. Power spectrum could reflect the energy change of EEG signal over a period of time, while EEG microstate could retain the energy of EEG signal on sub-second time scale. Based on this, we proposed a novel approach, using the abnormal frequency band of power spectrum as the frequency band for microstate analysis. Specifically, we employed deep neural network to obtain specific band ranges where the power spectra of the two groups significantly differed. Our results demonstrated that microstate analysis in the specific frequency band yielded high performance in explaining the variance of EEG data.

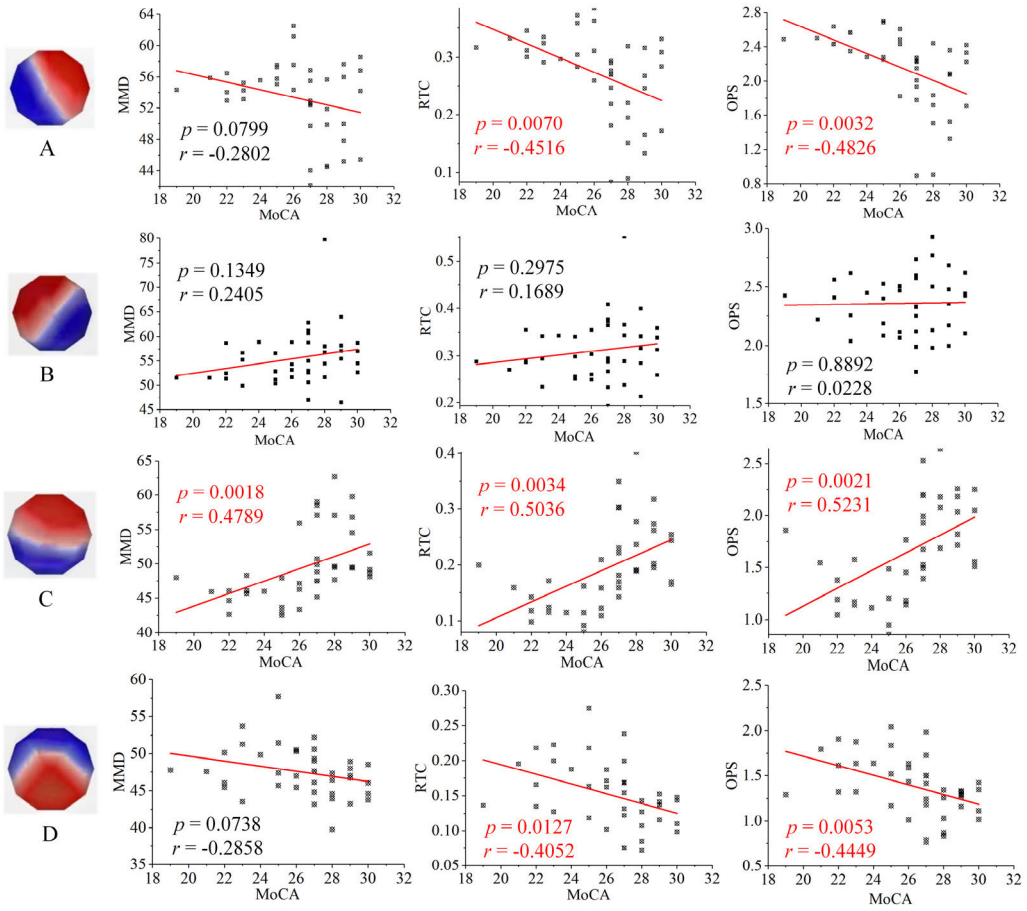

Fig. 6. Clinical MoCA correlations. Spearman correlations between microstate parameters of each microstate class and MoCA sores. R values are the slope of the fitting lines. For multiple comparisons, FDR correction is performed for *p* values. Each column represents each microstate parameters (Column 1: MMD; Column 2: RTC; Column 3: OPS). Each line represents each microstate classes (Line 1: A Class; Line 2: B Class; Line 3: C Class; Line 4: D Class;). For multiple comparisons, FDR correction acted on *p* values. Significant correlations are indicated by red font.

Unlike existing frequency band selection methods, our proposed approach does not rely on prior definitions, allowing for a more data-driven and objective approach.

The neuropathological mechanism of cognitive impairment in PD involves the pathological amyloid-beta, which is associated with a decline in cognitive ability [47]. Studies have suggested that beta-amyloid deposition in the brain initially occurs in the temporal lobe [44]. Another study observed abnormal microstate A parameters, such as increased duration and occurrence, which could potentially indicate underlying pathological changes in the temporal lobes, leading to disruptions in neuronal networks [36]. This observation suggests that the duration of microstate A could serve as a potent marker for cognitive impairment. Interestingly, our research revealed a significant increase in the occurrence and coverage of microstate A in ePD patients with MCI, consistent with previous studies [19]. Moreover, we observed a negative correlation between MoCA scores and the duration/coverage of microstate A, indicating that these parameters may effectively describe the cognitive levels of PD patients. Gschwind et al. proposed that the duration of microstate B was linked to cognitive fatigue in patients with multiple sclerosis [48]. However, our results did not show any abnormalities in microstate B, which aligns with our understanding that the characteristics of microstate patterns can differ based on the disease and its underlying cognitive impairments. Another study also reported a significant association between decreased duration of microstate C and cognitive decline in patients [49]. This finding aligns with our observations, indicating that as the cognitive level declined, the mean duration of microstate class C deviated from the normal level. Notably, the microstate D found in our study was similar to the class D in [18], where the subjects were all ePD patients. However, the microstate D found in Alzheimer's Disease and MCI [43] exhibited a different potential distribution compared to the microstate D found in ePD patients in our study. We inferred that cognitive impairment arising from different diseases influenced the microstate topology differently. According to Britz et al., the four microstates were associated with resting-state functional networks based on the blood-oxygen-level dependent (BOLD). Specifically, microstate D was interpreted as attention network [33]. Therefore, the increased duration, coverage and occurrence of microstate D in patients with MCI, as revealed in our work, suggested that the attention function may be abnormal in these individuals [50].

Overall, our previous work revealed unique microstate characteristics in ePD patients compared to healthy controls, investigating alterations in brain functional state dynamic.

This current work further divided the ePD group based on cognitive levels into ePD-MCI and ePD-nMCI, and explored the sub-second brain activity characteristics in ePD patients at different cognitive levels, providing valuable insights into the cognitive-related brain dynamics in ePD. However, there are still several limitations in this work. Firstly, the gender ratios in the ePD-MCI and ePD-nMCI groups were 6/7 and 6/21, respectively. Although the results of the chi-square test indicated no statistically significant difference in gender distribution between the two groups, a practical difference could be observed. Given that the non-statistical result might be due to the small sample size, we conducted additional subgroup analysis, the results of which are presented in the Supplementary Material, demonstrating that such gender distribution does not affect the main conclusions of this study. In the future, more participant data will be included so as to achieve a more balanced gender distribution and to further validate the generalizability of our findings. Secondly, during the process of frequency band optimization, while our method satisfied the requirements for deep learning applications, obtaining convincing results, the limited number of participants introduces the possibility that the different samples used in the training process and testing process may be from the same individuals. Since our cross-validation was conducted at the sample level, and the training and test sets could not guarantee complete separation at the individual level. In the future, utilizing a larger participant pool and conducting subject-level cross-validation can ensure complete separation of training and test sets at the subject level, further enhancing the credibility of our conclusion. Finally, the future work could employ higher spatial resolution EEG equipment for data collection to further examine the reliability of the findings presented in this research. These efforts will provide more comprehensive and robust evidence to support our findings and contribute to a better understanding of cognitive impairment dynamics in ePD patients.

V. Conclusion

A novel framework is proposed in this work to explore frequency-dependent microstate characteristics for ePD-MCI based on deep learning. A CNN model combined with the GRAD-CAM algorithm is utilized to identify the characteristic frequency band of ePD-MCI as 1-11.5Hz, achieving an ACC of 99.475% $\pm$ 0.3236% and an AUC of 99.495% $\pm$ 0.4400%. Using the characteristic frequency band, microstate analysis is carried out, and the dynamics of microstates are demonstrated to be correlated with the patients' cognition. Our results provide quantifiable signals for the early diagnosis of PD with cognitive impairment and offer insights into the pathogenesis of Parkinson's cognitive impairment. Meanwhile, the proposed research paradigm of frequency band optimization provides a new perspective for the selection of microstate frequency bands.

References

[1] J. Shi et al., "Cascaded multi-column RVFL+ classifier for single-modal neuroimaging-based diagnosis of Parkinson's disease," *IEEE Trans. Biomed. Eng.*, vol. 66, no. 8, pp. 2362–2371, Aug. 2019.

[2] P. Ren et al., "Gait rhythm fluctuation analysis for neurodegenerative diseases by empirical mode decomposition," *IEEE Trans. Biomed. Eng.*, vol. 64, no. 1, pp. 52–60, Jan. 2017.

[3] J. S. Schneider and S. Kortagere, "Current concepts in treating mild cognitive impairment in Parkinson's disease," *Neuropharmacology*, vol. 203, Feb. 2022, Art. no. 108880.

[4] E. R. Wallace et al., "Meta-analysis of cognition in Parkinson's disease mild cognitive impairment and dementia progression," *Neuropsychology Rev.*, vol. 32, no. 1, pp. 149–160, Mar. 2022.

[5] M. Broeders, R. M. A. de Bie, D. C. Velseboer, J. D. Speelman, D. Muslimovic, and B. Schmand, "Evolution of mild cognitive impairment in Parkinson disease," *Neurology*, vol. 81, no. 4, pp. 346–352, Jul. 2013.

[6] J. Pagonabarraga and J. Kulisevsky, "Cognitive impairment and dementia in Parkinson's disease," *Neurobiol. Disease*, vol. 46, no. 3, pp. 590–596, 2012.

[7] O. Monchi, A. Hanganu, and P. Bellec, "Markers of cognitive decline in PD: The case for heterogeneity," *Parkinsonism Rel. Disorders*, vol. 24, pp. 8–14, Mar. 2016.

[8] U. R. Acharya, S. L. Oh, Y. Hagiwara, J. H. Tan, H. Adeli, and D. P. Subha, "Automated EEG-based screening of depression using deep convolutional neural network," *Comput. Methods Programs Biomed.*, vol. 161, pp. 103–113, Jul. 2018.

[9] J. Schumacher et al., "Dysfunctional brain dynamics and their origin in lewy body dementia," *Brain*, vol. 142, no. 6, pp. 1767–1782, Jun. 2019.

[10] C. Chu et al., "Spatiotemporal EEG microstate analysis in drug-free patients with Parkinson's disease," *NeuroImage, Clin.*, vol. 25, Mar. 2020, Art. no. 102132.

[11] P. Milz, P. L. Faber, D. Lehmann, T. Koenig, K. Kochi, and R. D. Pascual-Marqui, "The functional significance of EEG microstates—Associations with modalities of thinking," *NeuroImage*, vol. 125, pp. 643–656, Jan. 2016.

[12] L. Tait et al., "EEG microstate complexity for aiding early diagnosis of Alzheimer's disease," *Sci. Rep.*, vol. 10, no. 1, Oct. 2020, Art. no. 17627.

[13] U. Smailovic et al., "EEG time signature in Alzheimer's disease: Functional brain networks falling apart," *NeuroImage Clin.*, vol. 24, Jan. 2020, Art. no. 102046.

[14] A. Pedroni, L. R. R. Gianotti, T. Koenig, D. Lehmann, P. Faber, and D. Knoch, "Temporal characteristics of EEG microstates mediate trial-by-trial risk taking," *Brain Topography*, vol. 30, no. 1, pp. 149–159, Jan. 2017.

[15] E. Santarnecchi et al., "EEG microstate correlates of fluid intelligence and response to cognitive training," *Brain Topography*, vol. 30, no. 4, pp. 502–520, Jul. 2017.

[16] J. I. Serrano et al., "EEG microstates change in response to increase in dopaminergic stimulation in typical Parkinson's disease patients," *Frontiers Neurosci.*, vol. 12, p. 714, Oct. 2018.

[17] H. Lian, Y. Li, and Y. Li, "Altered EEG microstate dynamics in mild cognitive impairment and Alzheimer's disease," *Clin. Neurophysiol.*, vol. 132, no. 11, pp. 2861–2869, Nov. 2021.

[18] E. Javed, P. Croce, F. Zappasodi, and C. D. Gratta, "Hilbert spectral analysis of EEG data reveals spectral dynamics associated with microstates," *J. Neurosci. Methods*, vol. 325, Sep. 2019, Art. no. 108317.

[19] C. S. Musaeus et al., "Changes in the left temporal microstate are a sign of cognitive decline in patients with Alzheimer's disease," *Brain Behav.*, vol. 10, no. 6, Apr. 2020, Art. no. e01630.

[20] B. T. Klassen et al., "Quantitative EEG as a predictive biomarker for Parkinson disease dementia," *Neurology*, vol. 77, no. 2, pp. 118–124, Jul. 2011.

[21] P. Polverino, M. Ajčević, M. Catalan, G. Mazzon, C. Bertolotti, and P. Manganotti, "Brain oscillatory patterns in mild cognitive impairment due to Alzheimer's and Parkinson's disease: An exploratory high-density EEG study," *Clin. Neurophysiol.*, vol. 138, pp. 1–8, Jun. 2022.

[22] L. C. Fonseca, G. M. A. S. Tedrus, P. N. Carvas, and E. C. F. A. Machado, "Comparison of quantitative EEG between patients with Alzheimer's disease and those with Parkinson's disease dementia," *Clin. Neurophysiol.*, vol. 124, no. 10, pp. 1970–1974, Oct. 2013.

[23] J. N. Caviness et al., "Differential spectral quantitative electroencephalography patterns between control and Parkinson's disease cohorts," *Eur. J. Neurol.*, vol. 23, no. 2, pp. 387–392, Feb. 2016.

[24] M. Hassan et al., "Functional connectivity disruptions correlate with cognitive phenotypes in Parkinson's disease," *NeuroImage, Clin.*, vol. 14, pp. 591–601, Dec. 2018.

[25] L. C. Yann et al., "Deep learning," *Nature*, vol. 521, no. 7553, pp. 436–444, May 2015.

[26] S. Zhu, T. Yang, and C. Chen, "Visual explanation for deep metric learning," *IEEE Trans. Image Process.*, vol. 30, pp. 7593–7607, 2021.

[27] R. Zhao et al., "Saliency detection by multi-context deep learning," in *Proc. IEEE Comput. Soc. Conf. Comput. Vis. Pattern Recognit. (CVPR)*, Jan. 2015, pp. 1265–1274.

[28] R. T. Schirrmeister et al., "Deep learning with convolutional neural networks for EEG decoding and visualization," *Human Brain Mapping*, vol. 38, no. 11, pp. 5391–5420, Nov. 2017.

[29] N. Vivaldi, M. Caiola, K. Solarana, and M. Ye, "Evaluating performance of EEG data-driven machine learning for traumatic brain injury classification," *IEEE Trans. Biomed. Eng.*, vol. 68, no. 11, pp. 3205–3216, Nov. 2021.

[30] D. P. Subha, P. K. Joseph, R. U. Acharya, and C. M. Lim, "EEG signal analysis: A survey," *J. Med. Syst.*, vol. 34, no. 2, pp. 195–212, Apr. 2010.

[31] R. G. de Peralta Menendez, M. M. Murray, C. M. Michel, R. Martuzzi, and S. L. Gonzalez Andino, "Electrical neuroimaging based on biophysical constraints," *NeuroImage*, vol. 21, no. 2, pp. 527–539, Feb. 2004.

[32] A. Pal, M. Behari, V. Goyal, and R. Sharma, "Study of EEG microstates in Parkinson's disease: A potential biomarker?" *Cognit. Neurodynamics*, vol. 15, no. 3, pp. 463–471, Jun. 2021.

[33] J. Britz, D. Van De Ville, and C. M. Michel, "BOLD correlates of EEG topography reveal rapid resting-state network dynamics," *NeuroImage*, vol. 52, no. 4, pp. 1162–1170, Oct. 2010.

[34] A. Khanna, A. Pascual-Leone, C. M. Michel, and F. Farzan, "Microstates in resting-state EEG: Current status and future directions," *Neurosci. Biobehavioral Rev.*, vol. 49, pp. 105–113, Feb. 2015.

[35] S. L. Oh et al., "A deep learning approach for Parkinson's disease diagnosis from EEG signals," *Neural Comput. Appl.*, vol. 32, pp. 10927–10933, Aug. 2020.

[36] C. S. Musaeus, M. S. Nielsen, and P. Høgh, "Microstates as disease and progression markers in patients with mild cognitive impairment," *Frontiers Neurosci.*, vol. 13, p. 563, Jun. 2019.

[37] R. R. Selvaraju, M. Cogswell, A. Das, R. Vedantam, D. Parikh, and D. Batra, "Grad-CAM: Visual explanations from deep networks via gradient-based localization," *Int. J. Comput. Vis.*, vol. 128, no. 2, pp. 336–359, Feb. 2020.

[38] G. Mostile et al., "Electrocortical networks in Parkinson's disease patients with mild cognitive impairment. The PaCoS study," *Parkinsonism Rel. Disorders*, vol. 64, pp. 156–162, Jul. 2019.

[39] J. N. Caviness et al., "Both early and late cognitive dysfunction affects the electroencephalogram in Parkinson's disease," *Parkinsonism Rel. Disorders*, vol. 13, no. 6, pp. 348–354, Aug. 2007.

[40] M. Y. Neufeld, S. Blumen, I. Aitkin, Y. Parmet, and A. D. Korczyn, "EEG frequency analysis in demented and nondemented parkinsonian patients," *Dementia Geriatric Cognit. Disorders*, vol. 5, no. 1, pp. 23–28, Jan. 1994.

[41] H. T. Jeong et al., "Power spectral changes of quantitative EEG in the subjective cognitive decline: Comparison of community normal control groups," *Neuropsychiatric Disease Treat.*, vol. 17, pp. 2783–2790, Sep. 2021.

[42] O. B. Simon et al., "Profiling Parkinson's disease cognitive phenotypes via resting-state magnetoencephalography," *J. Neurophysiology*, vol. 127, no. 1, pp. 279–289, Jan. 2022.

[43] V. L. Villemagne et al., "Longitudinal assessment of Aβ and cognition in aging and Alzheimer disease," *Ann. Neurol.*, vol. 69, no. 1, pp. 181–192, Jan. 2011.

[44] A. Widmann and E. Schröger, "Filter effects and filter artifacts in the analysis of electrophysiological data," *Frontiers Psychol.*, vol. 3, p. 233, Jan. 2012.

[45] J. Zulliger, L. Diaz Hernandez, and T. Koenig, "Within and between subject spectral fingerprints of EEG-microstate parameters," *Brain Topography*, vol. 35, no. 3, pp. 277–281, May 2022.

[46] A. Liang et al., "Treatment effect of exercise intervention for female college students with depression: Analysis of electroencephalogram microstates and power spectrum," *Sustainability*, vol. 13, no. 12, p. 6822, Jun. 2021.

[47] E. N. Wilson et al., "Soluble TREM2 is elevated in Parkinson's disease subgroups with increased CSF tau," *Brain*, vol. 143, no. 3, pp. 932–943, Mar. 2020.

[48] M. Gschwind et al., "Fluctuations of spontaneous EEG topographies predict disease state in relapsing-remitting multiple sclerosis," *NeuroImage, Clin.*, vol. 12, pp. 466–477, Feb. 2016.

[49] M. I. Tomescu et al., "From swing to cane: Sex differences of EEG resting-state temporal patterns during maturation and aging," *Develop. Cognit. Neurosci.*, vol. 31, pp. 58–66, Jun. 2018.

[50] A. Zarkali et al., "Visual dysfunction predicts cognitive impairment and white matter degeneration in Parkinson's disease," *Movement Disorders*, vol. 36, no. 5, pp. 1191–1202, May 2021.